AIP | Journal of Applied Physics

Thickness-dependent evolution of magnetization reversal in micron-scale polycrystalline Fe rings

Yu-feng Hou and Kannan M. Krishnan

Citation: J. Appl. Phys. **111**, 033910 (2012); doi: 10.1063/1.3681901
View online: http://dx.doi.org/10.1063/1.3681901
View Table of Contents: http://jap.aip.org/resource/1/JAPIAU/v111/i3
Published by the American Institute of Physics.

Thickness-dependent evolution of magnetization reversal in micron-scale polycrystalline Fe rings

Yu-feng Hou and Kannan M. Krishnan[a)]
Department of Materials Science, University of Washington, Seattle, Washington 98195, USA

(Received 30 November 2011; accepted 3 January 2012; published online 7 February 2012)

The evolution of magnetic switching mechanism is investigated for micron-scale polycrystalline Fe ring arrays with Fe layer thickness, t_{Fe}, varying between 10 nm and 50 nm. Single-step and double-step switching are observed for the 10 nm and 50 nm rings, with the 30 nm sample showing a transient behavior. As thickness increases, the first-step switching field, H_{c1}, increases, while the second-step switching field, H_{c2}, and remanent magnetization, M_r decreases. Magnetic force microscopy imaging and micromagnetic simulations reveal that in the reversal process, H_{c1} and H_{c2} correspond to the switching fields of two distinct halves of the ring. The relative separation between these two fields decides the switching behavior of the ring. © *2012 American Institute of Physics*. [doi:10.1063/1.3681901]

I. INTRODUCTION

Micron-scale ferromagnetic rings are currently the focus of intensive research because of their highly reproducible switching behavior and distinct magnetic states,[1,2] namely, the "onion" state with two opposite head-on domain walls,[3] which is attained reversibly from saturation; and the flux-closure or "vortex" state, in which the magnetization is oriented circumferentially around the ring, either clockwise or counterclockwise, without any domain walls.[4,5] The switching processes between these different magnetic states have been shown to be highly sensitive to the size,[6,7] width,[8] thickness,[9] and anisotropy[10] of the ring. Specifically, for micrometer-scale ferromagnetic rings with width larger than 500 nm, the transition between different states usually involves a local vortex nucleation step.[11,12] While there are a few studies on the different switching processes of ferromagnetic ring structures,[1,13,14] showing that the thick rings demonstrate a two-step reversal with vortex state formed between two saturated states[15] and the ultra-thin rings show a direct one step switching behavior,[16] yet so far, the continuous evolution process between these two different magnetization reversal mechanisms with the ring thickness, for a given diameter and width, is still not clear.

In this letter, micron-size polycrystalline Fe rings with systematic thickness variation were fabricated and the evolution of their magnetization reversal mechanism was studied using magneto-optical Kerr effect (MOKE) magnetometry, magnetic force microscopy (MFM), and micromagnetic simulations. Drastically different magnetic reversal processes are observed in the Fe rings as the thickness is systematically increased from 10–50 nm. MFM images obtained as a function of thickness and micromagnetic simulations performed to reveal the domain configurations of the Fe rings during the reversal processes are in good agreement.

[a)]Author to whom correspondence should be addressed. Electronic mail: kannanmk@uw.edu.

II. SAMPLE PREPARATION

A series of Ta (1 nm)/Cu (5 nm)/Fe (t_{Fe} nm)/Ta (3 nm) multilayer ring arrays with outer/inner diameter $d_{out}/d_{in} = 2.4\ \mu m/0.8\ \mu m$ and thickness, t_{Fe}, varying from 10 nm to 50 nm were fabricated on Si/SiO_2 substrate via a mask-transfer lithographic process, described elsewhere in detail.[17] The structure of the ring is shown in Fig. 1(a). The bottom Ta (1 nm)/Cu (5 nm) serves as a seed layer and the top Ta (3 nm) was deposited as a capping layer to prevent the whole structure from oxidation. Figure 1(b) shows scanning electron microscope images of the multilayer ring arrays and a detailed view of a single ring.

III. RESULTS AND DISCUSSION

A. Magneto-optical Kerr effect (MOKE) measurements

M-H hysteresis loops of the polycrystalline Fe rings were measured using a magneto-optical Kerr effect (MOKE) setup with external field applied in a longitudinal geometry at room temperature. To improve the signal-to-noise ratio, each loop was obtained by averaging the measured results over 20 times. Hysteresis loops of the 10 nm [Fig. 2(a)], 30 nm [Fig. 2(b)] and 50 nm [Fig. 2(c)] thick Fe ring samples were chosen to show the complete evolution process of hysteresis behavior with thickness. The first order derivative, dM/dH, of the descending branch is also plotted in the inset at the right bottom corner of each figure. The 10 nm loop shows a single-step transition from positive saturation to negative saturation, at the measured coercivity of $H_c = -75$ Oe. The distribution of the switching field is presented by the inset dM/dH curve, which shows one sharp peak at the coercive field, indicating the magnetization reversal is completed in one step. The 50 nm Fe ring [Fig. 2(c)] clearly shows a constricted shape with a two-step transition during magnetic reversal and a remanence state with no net magnetization, which is typical for the vortex state. The corresponding dM/dH plots show two well separated peaks. The first switching field $H_{c1} = 96$ Oe, corresponds to

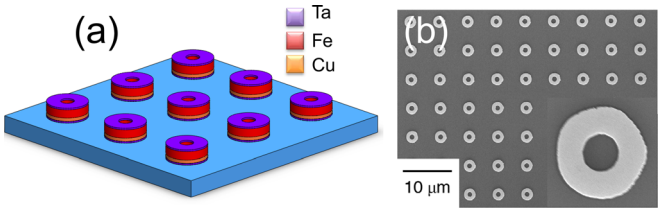

FIG. 1. (Color online) (a) Schematic structure of the polycrystalline Fe ring arrays. (b) Scanning electron microscopic images of the sample. A detailed image of one ring is shown on the bottom right corner.

the switching from the positive saturated state to the vortex state. The second switching field $H_{c2} = -262$ Oe, corresponds to the switching from vortex state to the reversed saturated state in the negative direction. In between these two switching steps, the vortex state is stable from −28 Oe to −152 Oe. The representative behavior between these two limiting cases of 10 nm and 50 nm is shown for a 30 nm ring in Fig. 2(b). The dM/dH curve of the descending branch shows two distinct peaks, yet these two peaks are partially overlapping, which indicates that the second reversal step is initiated before the completion of the first step, and without a stable vortex state formed in between. The variation of the remanent magnetization M_r/M_s and the value of the first and second switching fields as functions of the thickness for polycrystalline Fe rings are summarized in Fig. 2(d). The remanence ratio of the ring reduces from 0.88 for 10 nm to 0.02 for 50 nm, which shows a transition in magnetic state from the high magnetization quasi-uniform state to flux-closure vortex state. The first switching field H_{c1}, corresponding to the break of the positive saturated state, monotonically increases, indicating that with the increase in thickness, the quasi-uniform state is increasingly unstable at remanence. The field-separation between the first and second step switching, H_{c1}-H_{c2}, is increasing with thickness, which finally lead to the formation of the vortex state.

B. Magnetic force microcopy (MFM) imaging with applied field

The magnetic reversal process of the Fe rings was further investigated by MFM with the magnetic field applied parallel to the sample surface during scanning, and using 45 nm CoPt/FePt coated high coercivity probes with a lift height of 30 nm. Figure 3 shows MFM images of the 10 nm, 30 nm, and 50 nm ring samples measured at the nominal values of magnetic fields as marked in Figs. 2(a)–2(c). The corresponding applied field values of the MFM images were also marked in Fig. 3. As no significant asymmetry in the magnetization reversal is observed with increasing or decreasing field, we only display the images at different points of the descending branch. Figure 3(a) shows the MFM images of the 10 nm Fe rings varying from positive to negative saturation, corresponding to the descending branch in Fig. 2(a). In Fig. 3(a), 1, the applied field is +400 Oe, the ring is saturated in the positive direction, and black and white areas with dipolar contrast are observed at the edge of the ring along the external field direction, indicating the formation of the magnetic poles of opposite polarity in the saturated state. Parts 2 to 5 of Fig. 3(a) correspond to the applied field values of +200 Oe, 0 Oe, −200 Oe, and −400 Oe. As the field magnitude decreases, the spins start to relax to the local edge direction of the ring, causing the area of the dipolar contrast to shrink in size, as shown in Fig. 3(a), 2. At the remanent state [Fig. 3(a), 3], the ring still remains in the quasi-uniform state in the positive direction. It is after the field has changed its direction and surpasses H_{c1} that the dipolar contrast suddenly switches its direction, and the reversal is finished in one step [Fig. 3(a), 4]. At −400 Oe [Fig. 3(a), 5] the ring is saturated in the negative direction.

For the 30 nm Fe ring, the ring has the same saturated magnetic domain configuration at +400 Oe [Fig. 3(b), 6]. When the magnitude of the field decreases to H_{c1}, the first step of switching is initiated, as areas of black and white

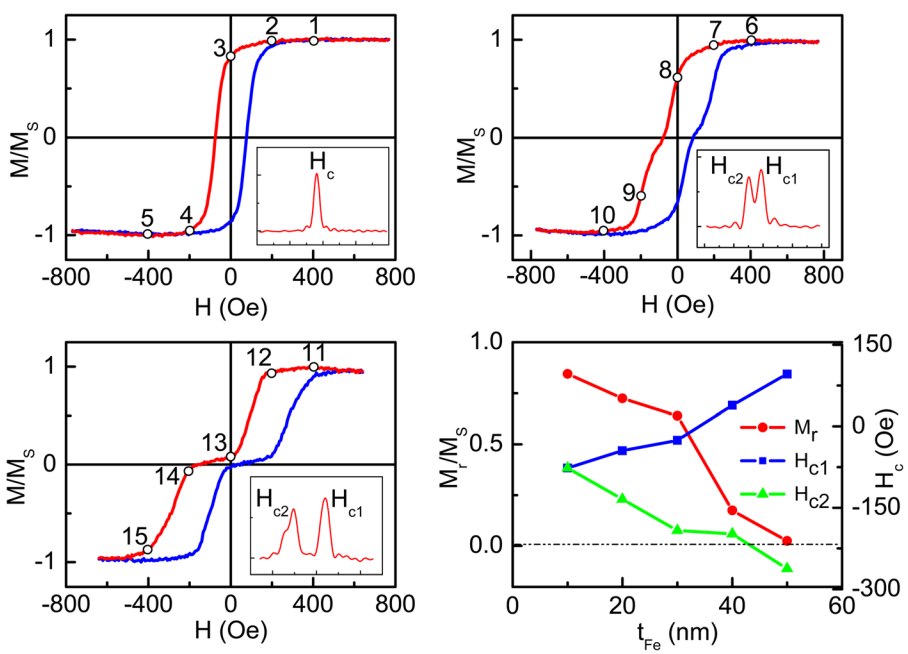

FIG. 2. (Color online) M-H hysteresis loops of (a) the 10 nm thick polycrystalline Fe ring arrays, (b) 30 nm thick polycrystalline Fe ring arrays, and (c) 50 nm thick polycrystalline Fe ring arrays; the first order derivative dM/dH of the loop's descending branch (red) are plotted in the inset box located at the right bottom corner of each loop. (d) The remanence magnetization M_r, first step switching field H_{c1}, and second step switching field H_{c2} as a function of the ring thickness t_{Fe}.

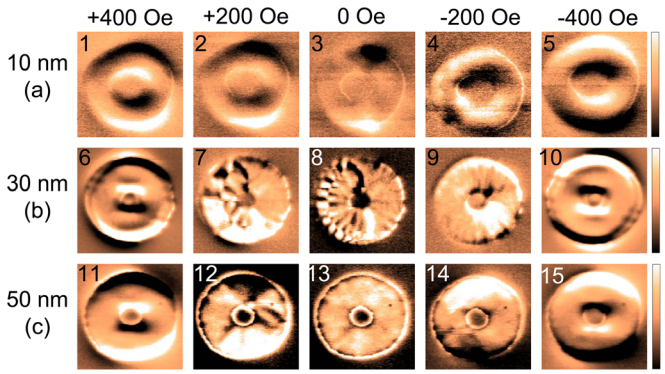

FIG. 3. (Color online) Selected MFM images showing the magnetic reversal process for (a) (1)–(5) the 10 nm thick polycrystalline Fe ring, (b) (6)–(10) the 30 nm thick polycrystalline Fe ring, and (c) (11)–(15)] the 50 nm thick polycrystalline Fe ring. All the MFM images were taken under the applied magnetic fields as marked at the top of the columns.

contrast were observed on the left half of the ring. However, no obvious contrast is observed on the right half of the ring, indicating that the magnetization direction remains in the circumferential direction. At remanence, as shown in Fig. 3(b), 8, while the magnetization in the right half of the ring is retained in its original circumferential direction, the left half of the ring, divided by two domains walls from the right half, starts to show the presence of vortex-antivortex chains in the form of alternating black-white contrast. This is consistent with earlier reports,[11] where they were also observed in the transient state from the saturated state to the formation of the vortex state. However, on further decreasing the field to −200 Oe, the vortex is not observed; instead, contrast starts to show on one half (right) of the ring [Fig. 3(b), 9], indicating the onset of the second switching step and the reversal of the magnetization on the right half of the ring via nucleation. Finally, as the field reaches −400 Oe, the ring gets saturated in the negative direction [Fig. 3(b), 10]. Thus, H_{c1} and H_{c2} correspond to the reversal of the left half and right half of the ring, respectively. However, between H_{c1} and H_{c2}, no stable vortex state was observed.

For the 50 nm ring, from the saturation state in the positive direction [Fig. 3(c), 11], the first switching step takes place on one half (right) of the ring via domain nucleation [Fig. 3(c), 12]. After the first step switching is completed, the magnetization direction of the right half is reversed to the circumferentially down direction and the ring forms the vortex state [Fig. 3(c), 13], as no magnetic contrast is observed. When the external field changes direction and reaches −200 Oe, the flux-closure state collapses and the magnetization of the other half (left) of the ring switches via nucleation [Fig. 3(c). 14]; when this nucleation is completed, the ring now gets saturated in the negative direction [Fig. 3(c), 15].

C. Micromagnetic simulation

Micromagnetic simulations of the magnetic reversal process of 10 nm, 30 nm, and 50 nm Fe rings have been performed using a Landau-Lifshitz-Gilbert micromagnetic solver.[18] The saturation magnetization and the exchange stiffness constant are set at the value of bulk Fe: $M_s = 1714\,\text{emu/cm}^3$ and $A = 12\,\mu\text{erg/cm}$. The cell size was set to be $5 \times 5 \times 5\ \text{nm}^3$.[19] In Fig. 4, the first row shows the simulated magnetization reversal process of the 10 nm sample, while the second and third rows show the results of the 30 nm and 50 nm sample, respectively. The local magnetization direction is indicated by the color wheel and the overlaid arrows. In Fig. 4(a), the 10 nm ring is magnetically saturated in the positive direction. As the magnitude of the field decreases, the spins at the edge of the ring starts to relax to the edge direction to minimize the stray field, as shown by the regions with magnetization pointing left and right at the edge of the ring in Fig. 4(b). At the remanence state, the ring still remains in the high remanent quasi-uniform state [Fig. 4(c)]. As the field changes direction and surpasses the coercivity, domains magnetized downward in the negative direction start to nucleate and grow [Fig. 4(d)] and finally, the ring saturates in the negative direction [Fig. 4(e)]. For the 30 nm rings, the initial state of the ring is also saturated in the positive direction [Fig. 4(f)]. As the magnitude of the field decreases, domains start to nucleate and grow on only one half (left) of the ring [Fig. 4(g)]. At remanence, the nucleation on the left half of the ring is not completed and a chain of vortex-antivortex cores is observed on this half of the ring; however, the spins on the right half of the ring almost remain unchanged. Further decreasing the field, the second step nucleation on the other half (right) of the ring starts while the nucleation on the left half is complete [Fig. 4(i)]. When the nucleation on the right half of the ring is also completed, the ring is saturated in the negative direction [Fig. 4(j)]. For the 50 nm ring, starting from the same saturated state in the positive direction [Fig. 4(k)], when the field decreases, the first step nucleation occurs on the left half of the ring and breaks it into a multi-domain state [Fig. 4(l)]. When the first step nucleation is completed, the magnetic spins on the left half of the ring are aligned circumferentially in the negative direction, while the spins on the right half are aligned circumferentially in the positive direction and the ring forms a perfect vortex state [Fig. 4(m)]. As the field decreases and reaches H_{c2}, the second step nucleation starts on the right half of the ring [Fig. 4(n)]. When the second step nucleation is finished, the ring forms a saturated state in the negative direction.

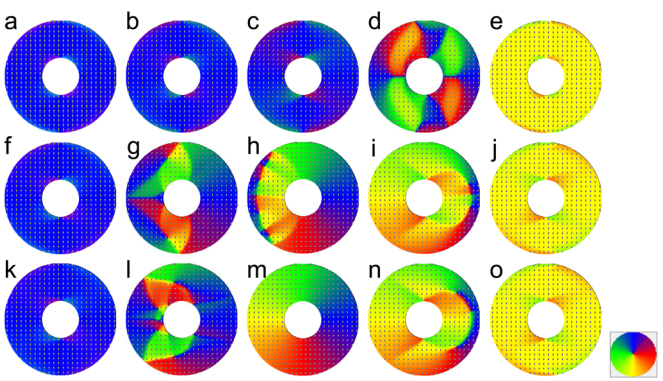

FIG. 4. (Color online) Micromagnetic simulated spin configurations of the 10 nm thick Fe ring in the magnetic reversal process (a)–(e), and the corresponding process for the 30 nm Fe ring (f)–(j) and 50 nm Fe ring (k)–(o). The magnetization direction is indicated by the color wheel or overlaid arrows.

IV. CONCLUSION

To qualitatively interpret the evolution of magnetization reversal process with thickness, H_{c1} and H_{c2} could be viewed as the switching fields for the two separate half-rings during the reversal process. As the external field is decreased from positive saturation, the first step switching is initiated and the magnetization of one half of the ring via domain nucleation (which half is decided by factors like edge roughness, defects, etc.) is reversed. When the first switching step is finished, the ring will form the vortex state. Further decreasing the field will trigger the second step switching, which reverses the magnetization of the other half of the ring. When the second step switching completes, the ring will get saturated in the negative direction. As the thickness of the ring, t_{Fe}, becomes smaller, the separation between the two switching fields, H_{c1}-H_{c2}, monotonically decreases [Fig. 2(d)], until there is no vortex state formation between these two steps (30 nm). For ultra-thin 10 nm samples, H_{c1}-H_{c2} has been reduced to zero and thus only one step switching is observed.

ACKNOWLEDGMENTS

The authors would like to thank Wei Zhang and Dr. M. Sheinfein, for help with the lithography and micromagnetic simulations, respectively. This work was supported by DOE/BES under Grant No. ER45987.

[1]M. Kläui, C. A. F. Vaz, L. J. Heyderman, U. Rudiger, and J. A. C. Bland, J. Magn. Magn. Mater. **290**, 61 (2005).
[2]C. A. F. Vaz, M. Kläui, L. J. Heyderman, C. David, F. Nolting, and J. A. C. Bland, Phys. Rev. B **72**, 224426 (2005).
[3]J. Rothman, M. Kläui, L. Lopez-Diaz, C. A. F. Vaz, A. Bleloch, J. A. C. Bland, Z. Cui, and R. Speaks, Phys. Rev. Lett. **86**, 1098 (2001).
[4]S. P. Li, D. Peyrade, M. Natali, A. Lebib, Y. Chen, U. Ebels, L. D. Buda, and K. Ounadjela, Phys. Rev. Lett. **86**, 1102 (2001).
[5]F. J. Castano, C. A. Ross, A. Eilez, W. Jung, and C. Frandsen, Phys. Rev. B **69**, 144421 (2004).
[6]S. D. Bader, Rev. Mod. Phys. **78**, 1 (2006).
[7]C. L. Chien, F. Q. Zhu, and J. G. Zhu, Phys. Today **60**, 40 (2007).
[8]M. Kläui, C. A. F. Vaz, L. Lopez-Diaz and J. A. C. Bland, J. Phys.: Condens. Matter **15**, R985 (2003).
[9]M. H. Park, Y. K. Hong, B. C. Choi, M. J. Donahue, H. Han, and S. H. Gee, Phys. Rev. B **73**, 094424 (2006).
[10]Y. F. Hou, Q. F. Zhan, and K. M. Krishnan, Appl. Phys. Lett. **98**, 042510 (2011).
[11]P. E. Roy, J. H. Lee, T. Trypiniotis, D. Anderson, G. A. C. Jones, D. Tse, and C. H. W. Barnes, Phys. Rev. B **79**, 060407(R) (2009).
[12]M. Kohda, K. Toyoda, T. Miyawaki, A. Fujita, and J. Nitta, J. Appl. Phys.**103**, 07A714(2008).
[13]C. A. F. Vaz, M. Kläui, J. A. C. Bland, L. J. Heyderman, C. David, and F. Nolting, Nucl. Instr. and Meth. in Phys. Res. B **246**, 13 (2006).
[14]S. P. Li, W. S. Lew, J. A. C. Bland, M. Natali, A. Lebib, and Y. Chen, J. Appl. Phys. **92**, 7397 (2002).
[15]F. J. Castano, C. A. Ross, C. Frandsen, A. Eilez, D. Gil, and H. I. Smith, M. Redjdal, and F. B. Humphrey, Phys. Rev. B **67**, 184425 (2003).
[16]Z. B. Guo, Y. K. Zheng, K. B. Li, Z. Y. Liu, P. Luo, and Y. H. Wu, J. Appl. Phys. **95**, 4918 (2004).
[17]W. Zhang, D. N. Weiss, and K. M. Krishnan, J. Micromech. Microeng. **21**, 045024 (2011).
[18]M. R. Sheinfein, the LLG code can be found at http://IIgmicro.home.mindspring.com/
[19]T. Miyawaki, K. Toyoda, M. Kohda, and A. Fujita, and J. Nitta, Appl. Phys. Lett. **89**, 122508 (2006).